Poster #: 7117

Convection Enhanced Delivery of a Novel ATR Inhibitor Synergizes With Systemic Lomustine For Improved Treatment of Glioblastoma

Alexander Josowitz[1,*], Teresa Lee[1,2,*], Ranjini K. Sundaram[2], Jinal Pothupitiya[1], Eric J. Brown[3,4], Amrita Sule[2], Jason Beckta[2], Yongheng Wang[1], Joseph Vacca[4], Oren Gilad[4], Ranjit S. Bindra[2], W. Mark Saltzman[1]

[1]Department of Biomedical Engineering, Yale University, New Haven, CT, [2]Department of Therapeutic Radiology, Yale University, New Haven, CT, [3]Perelman School of Medicine, University of Pennsylvania, Philadelphia, PA, [4]Aprea Therapeutics, Doylestown, PA

*These authors contributed equally

Yale University

APREA THERAPEUTICS

Introduction

Glioblastoma (GBM) is the most prevalent and deadly form of brain cancer, with a median survival of less than 15 months[1]. Despite a rigorous standard of care, including surgical resection and extensive concomitant radiotherapy with chemotherapy, the prognosis for GBM patients remains poor[2]. This is due to tumor recurrence, resistance to conventional therapies, pharmacokinetic challenges, and dose-limiting toxicities of existing therapies[3-4]. A major cause of resistance to the alkylator temozolomide (TMZ), the predominant chemotherapeutic agent used for GBM treatment, is increased activity of various DNA repair pathways[4]. Recent studies have shown that targeting DNA repair proteins, such as the ataxia telangiectasia and Rad3-related (ATR) kinase, alongside standard-of-care options is a promising anti-tumor strategy. ATR plays a crucial regulatory role in the DNA damage response and ATR inhibition has been shown to sensitize GBM tumors to both radiotherapy and chemotherapy[5-7]. Additionally, the alternative alkylator lomustine has demonstrated benefit in patients with recurrent, TMZ-resistant GBM[8-9].

In this study, we employ a combination approach using Aprea Therapeutics' next-generation macrocyclic ATR inhibitor, ATRN-333, to sensitize GBM tumors to alkylators. ATRN-333's macrocyclic structure allows for a rigid conformation, conferring greater selectivity for ATR and reducing off-target binding. We assess the ability of ATRN-333 to synergize with lomustine in GBM cell lines and in a murine flank tumor model. To overcome difficulties associated with drug delivery to the brain, we utilize a convection enhanced delivery (CED) system in conjunction with nanoparticle (NP) technology for direct intracranial administration of ATRN-333 to orthotopic GBM tumors, and examine the efficacy of this approach when combined with systemically administered lomustine.

Methods and Materials

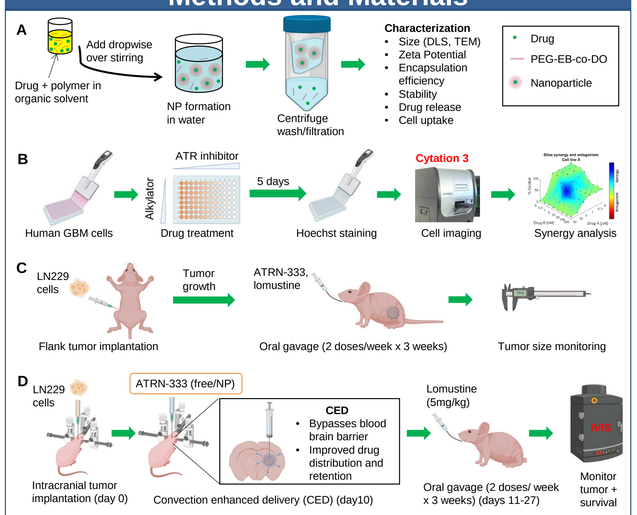

Protocols for investigating ATR inhibitor/alkylator combination therapy. (A) Formulation of drug into poly(ethylene glycol)-ethylene brassylate-co-1,4-dioxan-2-one (PEG-EB-co-DO) nanoparticles (NPs) using nanoprecipitation. (B) Cell viability combination assays using ATR inhibitors and alkylators in human GBM cell lines. (C) Assessment of ATRN-333 and lomustine efficacy in a flank tumor model. LN229 human glioma cells were implanted subcutaneously in female athymic Nude-Foxn1nu mice and ATRN-333 (free drug) and lomustine were administered orally. Tumor size was monitored using calipers. (D) Assessment of ATRN-333 and lomustine efficacy in an orthotopic GBM model. LN229 cells expressing Firefly luciferase were implanted into the brains of female athymic Nude-Foxn1nu mice. ATRN-333 (free or NP) was administered intracranially via convection enhanced delivery (CED), followed by oral administration of lomustine. Tumor size was monitored by bioluminescence imaging using an In Vivo Imaging System (IVIS).

1 PEG-EB-co-DO NPs demonstrate stability, sustained release, and effective uptake into glioma cells

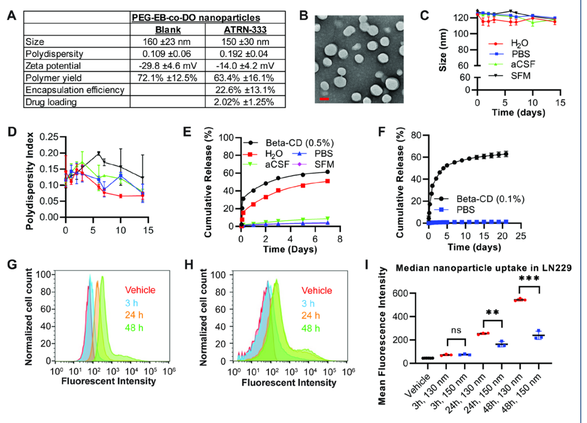

	PEG-EB-co-DO nanoparticles	
	Blank	ATRN-333
Size	160 ±23 nm	150 ±30 nm
Polydispersity	0.109 ±0.06	0.192 ±0.04
Zeta potential	-29.8 ±4.6 mV	-14.0 ±4.2 mV
Polymer yield	72.1% ±12.5%	63.4% ±16.1%
Encapsulation efficiency		22.6% ±13.1%
Drug loading		2.02% ±1.25%

Figure 1: (A) Physical characterization of blank and ATRN-333-loaded PEG-EB-co-DO NPs. (B) Transmission electron microscopy images of ATRN-333-loaded NPs, stained with Nano-W. Scale bar=100nm. (C, D) Hydrodynamic diameter (C) and polydispersity index (D) of ATRN-333-loaded PEG-EB-co-DO NPs over time in multiple media. N=3±SD. (E, F) Release of ATRN-333 from PEG-EB-co-DO NPs in various media over a 1 week (E) and 3 week (F) period. (G, H) Uptake of 150nm (G) and 130nm (H) DiD-loaded PEG-EB-co-DO NPs at different time points in human LN229 glioma cells, as measured by flow cytometry. (I) A comparison of fluorescence intensity between 130nm and 150nm NPs in LN229 cells at different time points. SFM, serum free media; aCSF, artificial cerebrospinal fluid; beta-CD, beta-cyclodextrin.

2 ATRN-333 potently inhibits ATR function in GBM cells

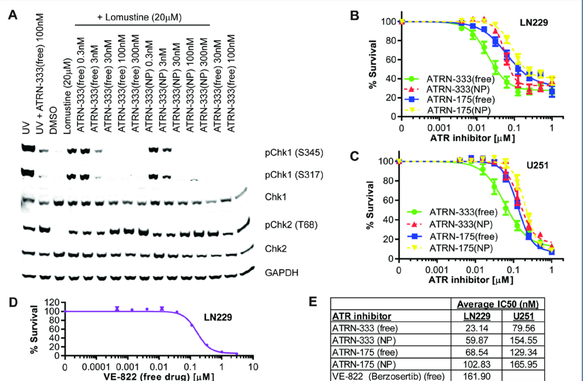

	Average IC50 (nM)	
ATR inhibitor	LN229	U251
ATRN-333 (free)	23.14	79.56
ATRN-333 (NP)	59.67	154.55
ATRN-175 (free)	68.54	129.34
ATRN-175 (NP)	102.83	165.95
VE-822 (Berzosertib) (free)	161.90	

Figure 2: (A) Western blot analysis of phospho-Chk1 and phospho-Chk2 levels in LN229 cells following treatment with vehicle, lomustine, or lomustine in combination with varying concentrations of ATRN-333 for 48 hours. UV treatment (100 J/m^2) is included as a DNA damage control. (B, C) Short term (5-day) viability assays in LN229 (B) and U251 (C) human GBM cells treated with the indicated ATRN analogs in free drug form or encapsulated with PEG-EB-co-DO. N=3±SEM. (D) Short-term viability assay in LN229 cells treated with VE-822. N=3±SEM. (E) Comparison of IC50 values for ATR inhibitors in LN229 and U251 cells, derived from cell viability assays in (B-D).

3 ATRN-333 synergizes with alkylators in LN229 cells

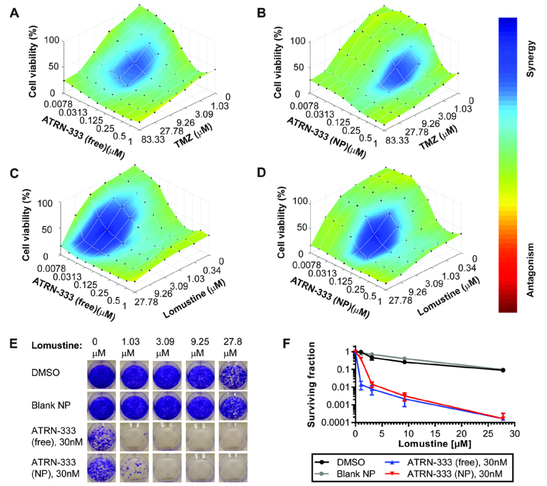

Figure 3: (A-D) Short-term (5-day) dose response cell viability assays for LN229 cells treated with ATRN-333 (free or NP) in combination with TMZ (A, B) or lomustine (C, D). Graphs were generated using Combenefit[10] and depict Bliss model synergy scores in color superimposed upon the three dimensional space. N=3. (E) Clonogenic survival assays in LN229 cells treated with lomustine and ATRN-333. Representative images are shown of LN229 cells stained with crystal violet after formation of colonies for 13 days. (F) Quantitation of the number of colonies in the treatment conditions shown in (E). N=3±SEM.

4 ATRN-333 sensitizes LN229 flank tumors to lomustine

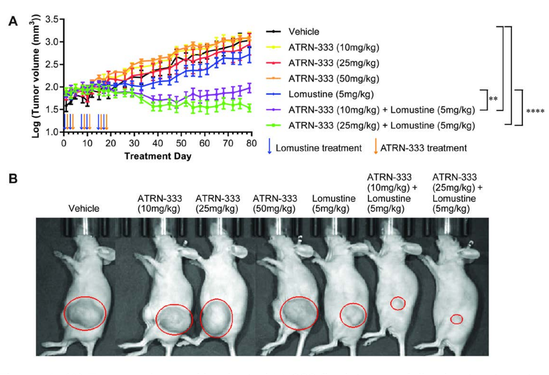

Figure 4: (A) Tumor volume of implanted LN229 flank tumors following treatment with ATRN-333, lomustine, or a combination of the two drugs. ATRN-333 (orange arrows) was delivered systemically either as a single agent or in combination with 5mg/kg lomustine (blue arrows). N=10±SEM. **P<0.01, ****P<0.0001. (B) Representative photographs showing flank tumors (circled in red) at the study's end.

5 ATRN-333 sensitizes LN229 intracranial tumors to lomustine

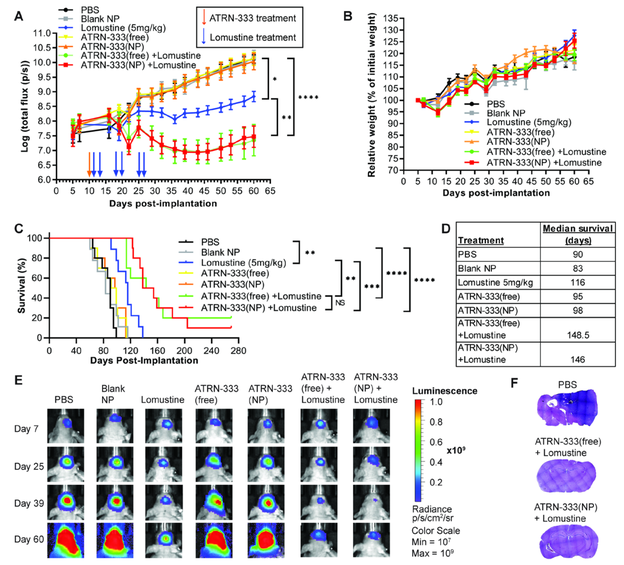

Figure 5: (A) Bioluminescence measurements of LN229 tumors implanted intracranially in athymic Nude-Fox1nu mice. ATRN-333 free drug and PEG-EB-co-DO NPs (orange arrows) were delivered intracranially via CED 10 days after tumor implantation, followed by systemic lomustine administration by gavage (blue arrows). (B) Relative weights of the mouse cohorts in (A). (C) Kaplan-Meier curves showing survival of mice with intracranial LN229 tumors and receiving the indicated treatments. (D) Median survival of cohorts presented in (A-C). N=9 or 10 ±SEM. *P<0.05, **P<0.01, ***P<0.001, ****P<0.0001, NS=not significant. (E) Representative bioluminescence images of LN229 tumors at various timepoints. (F) H&E staining of representative mouse brains from long-term survivors, compared to PBS control.

6 Toxicity and pharmacokinetic assessment of ATRN-333

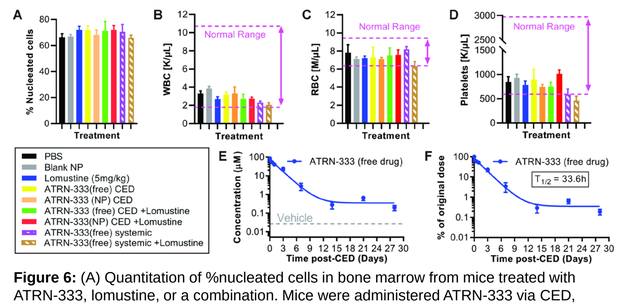

Figure 6: (A) Quantitation of %nucleated cells in bone marrow from mice treated with ATRN-333, lomustine, or a combination. Mice were administered ATRN-333 via CED, followed by 2 doses of lomustine orally, and sacrificed 5 days later. N=3±SEM. (B-D) Complete blood counts from the same cohorts of mice as (A). WBC, white blood cells; RBC, red blood cells. N=3±SEM. (E, F) ATRN-333 (free drug) levels in mouse brain tissue following CED administration, quantitated using LC-MS/MS. Data is presented as tissue concentration (E) and as a percentage of the injected dose (F). N=5±SEM.

Conclusions

ATRN-333 was successfully encapsulated into PEG-EB-co-DO polymeric NPs, which exhibited appropriate physicochemical properties for administration by CED to the brain. Both free and NP-encapsulated ATRN-333 showed high potency in inhibiting ATR function in cell-based assays. We demonstrated a clear synergistic effect between lomustine and ATRN-333 in GBM cell lines, and showed that ATRN-333 effectively sensitized both flank and intracranial tumors to lomustine *in vivo*. When administered via CED, ATRN-333 showed favorable intracranial retention and was well tolerated in mice when combined with lomustine. Our study demonstrates that ATR inhibitor/lomustine combination therapy, used in conjunction with a CED platform, is a powerful avenue for GBM treatment. These results support further investigation and potential clinical implementation of ATRN-333 and other macrocyclic ATR inhibitors as chemosensitizers for GBM.

Acknowledgements

Brain tissue processing and subsequent LC-MS/MS analysis for the pharmacokinetic study was performed by WuXi AppTec. Paraffin-embedding, sectioning, and H&E staining of tissues was performed by the Yale Pathology Tissue Services (YPTS) core facility.

References

1. Alifieris, C., and Trafalis, D.T. (2015). *Pharmacol Ther* **152**:63-82.
2. Stupp R., Hegi, M.E., Mason, W.P., *et al.* (2009). *Lancet Oncol.* **10(5)**:459-66.
3. Milano, M.T., Okunieff, P., Donatello, R.S., *et al.* (2010). *Int J Radiat Oncol Biol Phys.* **78(4)**:1147-55.
4. Lee, S.Y. (2016). *Genes Dis* **3**:198-210.
5. Jackson, C.B., Noorbakhsh, S.I., Sundaram, R.K., *et al.* (2019). *Cancer Res* **79**:4331-4338.
6. Chen, E.M., Quijano, A.R., Seo, Y.E., *et al.* (2018). *Biomaterials* **178**:193-203.
7. King, A.R., Corso, C.D., Chen, E.M., *et al.* (2017). *Mol Cancer Ther* **16**:1456-1469.
8. Herrlinger, U., Tzaridis, T., Mack, F., *et al.* (2019). *Lancet* **393**:678-688.
9. Yamamuro, S., Takahashi, M., Satomi, K., *et al.* (2021). *Cancer science* **112**:4736-4747.
10. Di Veroli, G.Y., Fornari, C., Wang, D., *et al.* (2016). *Bioinformatics* **32**:2866-2868.